ARTICLE IN PRESS



Available online at www.sciencedirect.com

ScienceDirect

Geochimica et Cosmochimica Acta xxx (2022) xxx-xxx

Geochimica et Cosmochimica

www.elsevier.com/locate/gca

U_{38ME} Expands the linear dynamic range of the alkenone sea surface temperature proxy

Joseph Novak ^{a,b}, Sarah M. McGrath ^a, Karen Jiaxi Wang ^{a,c}, Sian Liao ^{c,d}, Steven C. Clemens ^a, Wolfgang Kuhnt ^e, Yongsong Huang ^{a,c,*}

a Department of Earth, Environmental and Planetary Sciences, Brown University, Providence, RI 02912, USA
 b Ocean Sciences Department, University of California, Santa Cruz, CA 95064, USA
 c Institute at Brown for Environment and Society, Brown University, Providence, RI 02912, USA
 d Department of Chemistry, Brown University, 324 Brook Street, Providence, RI 02912, USA
 c Institute of Geosciences, Kiel University, Ludwig-Meyn-Str. 10-14, 24118 Kiel, Germany

Received 30 July 2021; accepted in revised form 19 April 2022; available online xxxx

Abstract

The alkenone paleothermometer, $U_{37}^{K'}$, has been used to estimate past sea surface temperatures (SST) for nearly forty years. Despite its popularity, $U_{37}^{K'}$ is conventionally limited to water temperatures between 5 and 28.5 °C. At both low and high temperature ranges [0-8; >24 °C], $U_{37}^{K'}$ displays nonlinear behavior and significant scattering, leading to major uncertainties in reconstructed SSTs. With data from 171 surface sediments across the global ocean, we demonstrate that $U_{38ME}^{K'}$, an unsaturation index based on the ratio of di and tri unsaturated methyl alkenones with 38 carbon atoms ($C_{38}ME$), extends the linear dynamic range of alkenone SST estimates from 0 to 29.5 °C SST. Accurate measurements of $U_{38ME}^{K'}$ are made possible by recent advances in chromatographic techniques that provide excellent resolution of C_{38} alkenones, as well as improved separation of all alkenone homologues. Our newly calibrated $U_{38ME}^{K'}$ permits more accurate SST reconstruction in warmer ocean waters and climates. $U_{38ME}^{K'}$ also carries less risk than $U_{37}^{K'}$ of biased SST estimates in regions (e.g. estuaries, closed seas) where both open ocean and coastal alkenone producers (e.g., *Isochrysis galbana*) are present because the latter do not produce C_{38} methyl ketones but do produce C_{37} methyl ketones. The efficacy of the $U_{38ME}^{K'}$ paleothermometer is shown by downcore analyses of early Pliocene age sediments from ODP sites 806 and 1143, as well as Holocene age sediments from the Black Sea. The $U_{38ET}^{K'}$ paleothermometer is also evaluated and found to be unsuitable for paleoceanographic applications.

Keywords: Alkenones; Paleothermometer; $U_{37}^{K'}$; $U_{38MF}^{K'}$

1. INTRODUCTION

Paleo sea surface temperature (SST) reconstructions are vital for understanding the Earth climate system. Paleo SSTs are studied through a variety of proxies such as cer-

E-mail address: yongsong huang@brown.edu (Y. Huang).

https://doi.org/10.1016/j.gca.2022.04.021 0016-7037/© 2022 Elsevier Ltd. All rights reserved. tain coccoliths through their production of alkenones (Prahl and Wakeham, 1987; Müller et al., 1998; Conte et al., 2006; Tierney and Tingley, 2018), producers of isoprenoid glycerol dialkyl glycerol tetraethers (Schouten et al., 2002; Tierney and Tingley, 2014), and planktonic foraminifera through faunal assemblage analyses via transfer functions (Imbrie and Kipp, 1971; Kucera et al., 2005), and the calcite δ^{18} O (Urey, 1947; Epstein et al., 1953; Erez and Luz, 1983; Malevich et al., 2019) and Mg/Ca (Nürnberg et al., 1996; Elderfield and Ganssen, 2000;

^{*} Corresponding author at: Department of Earth, Environmental and Planetary Sciences, Brown University, Providence, RI 02912, USA.

Dekens et al., 2002; Anand et al., 2003; Tierney et al., 2019b) ratios of their tests. Multiple factors complicate the various paleotemperature proxies, including subsurface habitats of the organism(s) (Karner et al., 2001; Telford et al., 2013; Hernández-Sánchez et al., 2014), productivity-dependent depth habitat of the organism(s) (Lawrence et al., 2020), the carbonate ion concentration of seawater (Spero et al., 1997; Russell et al., 2004), the preservation of foraminifera tests in deep oceans, and other nonthermal factors (Shackleton, 1987; Zhang et al., 2016).

The alkenone paleothermometer is unique in the field of oceanography because the influence of nonthermal environmental factors such as nutrient availability, alkenone degradation, and lateral advection is thought to be relatively small on paleotemperature estimates in most ocean settings (Epstein et al., 1998; Herbert, 2001, 2003; Prahl et al., 2003, 2010; Ausín et al., 2021). The alkenone SST proxy is traditionally based on the alkenone producers' growth temperature-dependent ratio of di-unsaturated and triunsaturated 37-carbon methyl-ketones $(U_{37}^{K'})$ (Prahl and Wakeham, 1987), which has been calibrated to SST in the water column (Conte and Eglinton, 1993; Sikes and Volkman, 1993; Conte et al., 1994, 2001, 2006; Ternois et al., 1997; Sicre et al., 2002; Bendle and Rosell-Melé, 2004), lab-grown cultures (Conte et al., 1998; Epstein et al., 1998; Prahl et al., 1988; Sawada et al., 1996; Volkman et al., 1995; Yamamoto et al., 2000), and core top sediments (Sikes et al., 1991; Rosell-Melé et al., 1995; Müller et al., 1998; Conte et al., 2006; Prahl et al., 2010; Tierney and Tingley, 2018). $U_{37}^{K'}$ is bounded between 0–1, which corresponds to approximately 0-30 °C, depending on calibration applied (Müller et al., 1998; Tierney and Tingley, 2018). $U_{37}^{K'}$ is restricted to open-ocean depositional environments due to the occurrence of endemic alkenoneproducing coastal haptophytes (Mercer et al., 2005; Bendle et al., 2009; Kaiser et al., 2019).

Nonlinearity in the $U_{37}^{K'}$ calibration has been observed in culture (Conte et al., 1998), water column (Sikes and Volkman, 1993; Bentaleb et al., 2002; Conte et al., 2006; Gould et al., 2017), sediment trap (Goni et al., 2001; Richey and Tierney, 2016), and core top (Sonzogni et al., 1997) studies. The Bayesian b-spline (BAYSPLINE) calibration (Tierney and Tingley, 2018) is a new attempt to model the high-temperature extreme of the $U_{37}^{K^\prime}$ calibration. Importantly, the BAYSPLINE calibration characterizes slope attenuation of the SST- $U_{37}^{K'}$ relationship as it reaches saturation ($U_{37}^{K'} = 1$) around 30 °C (Tierney and Tingley, 2018). Constraining the behavior of $U_{37}^{K'}$ as SST approaches 0 °C remains a challenge because abnormally high $U_{37}^{K'}$ values in the northern hemisphere high latitudes (Tierney and Tingley, 2018; Max et al., 2020), especially where seasonal sea ice is present (Filipova et al., 2016; Tierney and Tingley, 2018; Wang et al., 2021), limit the effective sampling area for SSTs < 5 °C. These seasonality biases may have resulted from two processes: (1) the imprint of higher autumnal alkenone flux on the alkenone SST signal, as observed north of the Subarctic Front in the North Pacific (Harada et al., 2006; Seki et al., 2007; Max et al., 2020); (2) the co-occurrence of Group 2i Isochrysidales in regions with seasonal sea ice cover (Wang et al., 2021). The temperature-dependence of C_{37} alkenone production in Group 2i Isochysidales is likely radically different from those in the Group 3 marine haptophytes *Emiliania huxleyi* and *Gephyrocapsa oceanica*, as demonstrated in culture experiments (Zheng et al., 2019; Wang et al., 2021). Despite over three decades of study, the reasons for the substantial scatter in the $U_{37}^{K'}$ calibration below 5 °C and above 28 °C remain elusive (Tierney and Tingley, 2018).

Compared to the C₃₇ ketones, C₃₆, C₃₈, and C₃₉ alkenones and alkenoates have received much less attention. $U^{K^{'}}$ indices based on the C_{38} alkenones, $U^{K'}_{38ME}$ and $U^{K'}_{38ET},$ were originally proposed by Conte and Eglinton (1993) based on suspended particulate matter (SPM) collected from the water column. Conte et al. (1998) later measured $U_{38ME}^{K'}$ and $U_{38ET}^{K'}$ in cultures of $\emph{E. huxleyi}$ and $\emph{G. oceanica}$. Subsequent comparison of $U_{38ME}^{K'}$ and $U_{37}^{K'}$ measured in sediment cores from the California Margin demonstrated strong, positive covariance of the two indices to at least the late Pliocene (Herbert, 2003). However, C₃₈ alkenones were ultimately discarded for use as an SST proxy mainly due to analytical difficulties (see Herbert, 2001). Specifically, the nonpolar GC columns in use at the time (e.g. the HP-1 or DB-1 column) provided poor resolution of the 2 and 3 double bond 38-carbon methyl ketones (C₃₈ME) and 38-carbon ethyl ketones (C₃₈ET), causing significant uncertainties in quantification of their relative abundances due to coelution, especially at extreme temperatures when a small peak coelutes with a large peak in gas chromatograms (see Kaiser et al., 2019, for further reading). Longo et al. (2013) were the first to resolve this issue with use of the VF-200 mid-polarity poly(trifluoropropylme thylsiloxane) GC column. This work was later improved upon by Zheng et al. (2017), who achieved complete separation of C₃₈ and C₃₉ alkenones by use of the RTX-200 mid-polarity poly(trifluoropropylmethylsiloxane) GC column.

Recent work has demonstrated a strong relationship of $U_{38\text{ME}}^{K'}$ to growth temperature in both algal culture (Zheng et al., 2019) and SPM (Zheng et al., 2019) that, when extrapolated to $U_{38\text{ME}}^{K'} = 1$, could reach saturation at temperatures of ~ 32.2 °C (culture) and ~ 31.4 °C (SPM) due to an offset in the calibration equation's intercept relative to $U_{37}^{K'}$. Thus, depending on temperature, the ratio of triunsaturated to di-unsaturated alkenones is ca. 53.2–14.3% higher in C_{38} ME than C_{37} methyl ketones. This suggests that $U_{38\text{ME}}^{K'}$ may extend alkenone paleotemperature determinations to new upper temperature limits. Building on this work, we present the first global core top calibration of $U_{38\text{ME}}^{K'}$

The main objectives of this study are (1) to calibrate $U_{38\text{ME}}^{K'}$ measured in surface sediments from global sites that represent a range of mean annual SSTs from -1 to 29.5 °C. We are particularly interested in observing the relationship between $U_{38\text{ME}}^{K'}$ and SST above 24 °C to determine whether the same nonlinear behavior reported in the $U_{37}^{K'}$ calibration

is present with $U_{38ME}^{K'}$. (2) to use simultaneous measurements of $U_{38ME}^{K'}$ and $U_{37}^{K'}$ in Pliocene age sediments from the Indo-Pacific Warm Pool to ascertain whether $U_{38ME}^{K'}$ behaves differently than $U_{37}^{K'}$ at SSTs warmer than those observed in the contemporary ocean. We consider this question especially important since we hypothesize that $U_{38ME}^{K'}$ would be particularly effective for studying past warm climates.

2. MATERIAL AND METHODS

2.1. Surface sediments

We measured C_{37-8} alkenones in 167 core tops (N = 66 Atlantic, N = 73 Pacific, N = 32 Indian) that span a mean annual SST range from -1 to 29.5 °C (Fig. 1, Supplementary Table 1). To ensure high data quality for our SST calibrations, all core tops sampled were multicores or box cores from the 0–7 cm or shallower depth range and 96% of the core tops are from the 0–3 cm or shallower depth interval. Multicore and box core samples were chosen specifically because of their superior preservation of the sediment-water interface during sample collection (Jahnke and Knight, 1997; Tuit and Wait, 2020). The core tops represent an area from 76.75°N–76.5°S and 178.8E–179.6 W (Fig. 1). 4 core top samples from Kaiser et al. (2019) were also included for a total of 171 core tops considered in the $U_{3\text{NME}}^{K'}$ calibration.

2.2. Oceanographic data

Core tops were assigned mean annual SST values (0 m depth) from the National Oceanic and Atmospheric Administration (NOAA) Optimum Interpolation Sea Surface Temperature (OISST) 0.25° gridded product, which is based on a combination of ship, buoy, and satellite observations (Banzon et al., 2016). Core top samples were assigned the SST value of the closest point on the grid to the core top location. The proximity of core top samples to sea ice was determined by calculating mean annual sea

ice concentration from 1979–2020 from the National Snow and Ice Data Center (NSIDC) Climate Data Record of Passive Microwave Sea Ice Concentration, Version 3, with a spatial resolution of 25 km × 25 km (Peng et al., 2013; Meier et al., 2017), and by comparison of sample locations to regional sea ice charts (Parkinson and Gratz, 1983; Mysak and Manak, 1989; Divine and Dick, 2006; Smith and Comiso, 2008).

2.3. Sample preparation and analysis

2.3.1. Sediment storage

Between 1 and 15 g of sediment samples were shipped from sediment repositories in unrefrigerated boxes to Brown University. Upon receiving shipment, samples were frozen until freeze dried.

2.3.2. Sample extraction

Freeze dried sediment was ground with a mortar and pestle and mixed with baked sand. Ground samples were extracted using a 9:1 dichloromethane:methanol (DCM: MeOH) mixture in an ASE-200. The extraction program on the ASE-200 was set to 3 20-minute static cycles run at 120 °C and 1200 psi.

2.3.3. Silica gel chromatography

Total lipid extracts (TLE) were dissolved in 1 mL hexane and eluted onto a silica gel flash column (230–400 mesh, 40–63 µm, 60 Å pore size from Silicycle Inc.), followed by elution of the alkane fraction by an additional 3 mL of hexane into a 4 mL vial. The ketone fraction was eluted by 4 mL DCM and collected in a second vial. A subset of samples was then dried under N_2 gas, transferred to a 100uL insert in a 2 mL vial, and analyzed on GC-FID according to the method below. It became apparent that most samples would require further cleaning, so there was no further analysis of samples prepared only by silica gel.

2.3.4. Silver nitrate chromatography

It was quickly realized that more tedious preparation steps are required for analysis of $U^{K'}_{38ME}$ than $U^{K'}_{37}$ because

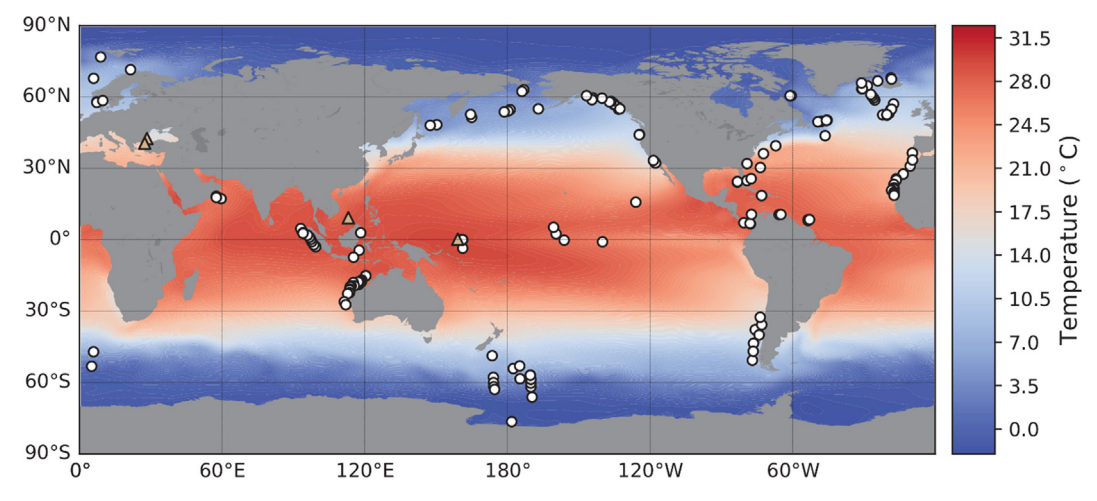


Fig. 1. Map of core top sites sampled in this study (n = 171). Sites are represented by black dots. Tan triangles mark ODP sites 806 and 1143 in the Pacific Ocean as well as sediment cores GGC18 and GeoTü in the Black Sea and Sea of Marmara.

38-carbon methyl alkenones are, on average, only 30% as abundant as their 37-carbon methyl alkenone counterparts in our samples (Supplementary Figs. S1, S2). In practice, this means that reliable quantification of $U_{38ME}^{K'}$, especially as $U_{38ME}^{K'}$ approaches 0 or 1, requires thorough elimination of interfering compounds, as the quantity of tri or di unsaturated C₃₈ME alkenone present is very small. Methods for purifying alkenones according to double bond numbers (D'Andrea et al., 2007; Dillon et al., 2016) or isolating both alkenones and alkenoates (Wang et al., 2019) using argentation chromatography have been previously published. While these methods provide excellent separation of alkenones, the use of mixed solvents entails significant sample preparation time. In this study, due to the need to analyze many samples, we developed an argentation chromatography that uses only pure solvents and provides adequate cleaning of samples for accurate measurements of alkenone unsaturation ratios. Ketone fractions separated by the silica gel flash column were dissolved in ~1 mL DCM and eluted onto a silver nitrate (0.6 g silver nitrate-impregnated silica gel, 10 weight %, 200 + mesh from SigmaAldrich) flash column, followed by an additional 3 mL DCM. The fraction that contained alkenones with 2 to 4 double bonds was then collected in two 4 mL vials by elution of 8 mL of ethyl acetate. The alkenone fraction was dried under N₂ gas and combined in a 100 µL insert in a 2 mL vial before analysis on GC-FID according to the method below. Prior work has shown complete retention of alkenones by 2.1 g of silver nitrate impregnated silica gel after elution with 20 mL of DCM (D'Andrea et al., 2007). This method has been successfully used on lacustrine alkenone samples (Richter et al., 2020).

2.3.5. Saponification reaction

Further cleaning by saponification was performed on 114 samples to remove any wax esters that could coelute with alkenones. Saponification was only performed after initial analysis by GC-FID after the silver nitrate argentation chromatography step. Samples were dissolved in ~1 mL KOH solution in a 4 mL vial which was then capped and shaken to ensure complete dissolution of organics. KOH solution was prepared by dissolution of 5.61 g of KOH in a 95:5 MeOH:H₂O solution made with Milli-Q purified water. The vials were heated for 3 hours in a heating block at 65 °C. After the first half-hour, the vials were vented and shaken. The samples were then allowed to cool to room temperature before ~1 mL of NaCl solution was added to the samples. The NaCl solution was prepared by mixing 15 g NaCl with 285 mL of Milli-Q purified water. 1 mL hexane was then added to the samples for liquid-liquid extraction. The alkenone fraction was then dried and dissolved in DCM before elution on a silica column to remove any salts.

2.3.6. GC-FID analysis

Samples were analyzed by gas chromatography-flame ionization detection Agilent 7890 N Series instrument with splitless injection and Restek Rtx-200 ms (105 m \times 250 $\mu m \times$ 0.25 $\mu m)$ poly(triflouropropylmethylsi

loxane) stationary phase semi-polar column (Zheng et al., 2017). Helium carrier gas flow rate of the GC-FID was set to 1.5 mL/min. The GC oven program was as follows. Initial temperature of 50 °C was held for 2 min, then ramp 20 °C/min to 255 °C followed by ramp 3 °C/min to 320 °C which was then held for 25 min. This method was chosen to fully separate C₃₈ methyl and ethyl alkenones. Peaks were quantified using the MATLAB chromatography toolbox GUI program developed by Dillon and Huang (2015). Peak areas were calculated by using the exponential gaussian hybrid function, which calculated peak area based on the raw data rather than the curve fit to the data. Individual C₃₇-C₃₉ alkenones were identified based on the elution time of alkenones in a laboratory sediment standard, which were used as reference for the chromatography toolbox's automatic peak picking function. Occasionally, it was necessary to manually repick peaks to correct errors made by the automatic peak picking function. In these cases, elution times of alkenones in samples were manually compared to the elution times of alkenones in the most recently analyzed sediment standard.

2.4. Statistical analyses

Ordinary least-squares regression was performed using the 'lm()' function in R. The 'lm()' function derives R² and p-values from the Pearson correlation, which is significant when the p-value is less than 0.05. The Shapiro-Wilkes test for normality (Shapiro and Wilk, 1965) was performed using the 'shapiro.test' function in R. In cases where distributions fail the Shapiro-Wilkes test, the more general Kolmogorov-Smirnov test was used to test whether the data fit Student's t distribution (Massey, 1951). This was done with the 'ks.test()' function in R, which was used to compare the data to a hypothetical t-distribution with the same mean and standard deviation of the data in question. The hypothetical t-distribution was generated with the 'dt()' function. Outliers in our $U^{K'}_{38ME},~U^{K'}_{37},$ and, $\frac{C_{38}ME}{C_{38}ET}$ datasets were identified by the Rosner test using the 'rosnerTest()' function in the 'EnvStats' package in R as in the recent global lacustrine brGDGT temperature calibration (Rosner, 1983; Millard and Kowarik, 2018; Martínez-Sosa et al., 2021). In all cases, the suspected number of outliers, k, was set to 10.

2.5. Calculation of alkenone indices

 $U^{K^{'}}$ indices were calculated for C_{37} and C_{38} alkenones according to the formulae below.

$$U_{37}^{K'} = C_{37;2ME} / (C_{37;2ME} + C_{37;3ME})$$
 (1)

(Prahl and Wakeham, 1987).

$$U_{38ME}^{K'} = C_{38:2ME} / (C_{38:2ME} + C_{38:3ME})$$
 (2)

(Conte and Eglinton, 1993).

$$U_{38\text{ET}}^{K'} = C_{38:2\text{ET}} / (C_{38:2\text{ET}} + C_{38:3\text{ET}})$$
(Conte and Eglinton, 1993).

2.6. Age models

The ODP site 806 age model is based on biostratigraphic datums (Chaisson and Leckie, 1993). The ODP site 1143 age model is based on an orbitally tuned benthic foraminifera oxygen isotope record (Tian et al., 2002). Core GGC18 from the Black Sea and core GeoTü from the Sea of Marmara have age models based on radiocarbon dates (Sperling et al., 2003; Huang et al., 2021).

3. RESULTS

All calibration equations are summarized in Table 1.

3.1. Regression of $U_{38ME}^{K^{\prime}}$ to sea surface temperature

Ordinary least squares regression of our $U_{38\text{ME}}^{K'}$ data to annual SST yielded a strong positive relationship ($R^2=0.964,\ p\ll0.001,\ RMSE=1.84\ ^{\circ}\text{C},\ n=171,$ Fig. 2a) where $U_{38\text{ME}}^{K'}$ is related to mean annual SST by the equation:

$$U_{38ME}^{K'} = SST * 0.031 + 0.056 \tag{4}$$

There are 15 samples in both the $U_{38ME}^{K'}$ and $U_{37}^{K'}$ datasets from regions with sea ice (Fig. 2a, b). These samples were removed from the dataset due to the association of large positive $U_{37}^{K'}$ residuals with the presence of sea ice in the

high latitude Atlantic and Pacific and the documented production of C_{38} methyl alkenones by Group 2i sea ice associated haptophytes in culture (Filipova et al., 2016; Tierney and Tingley, 2018; Wang et al., 2021). The remaining samples were regressed to mean annual SST, which yields the equation:

$$U_{38ME}^{K'} = SST * 0.032 + 0.016 (5)$$

with $R^2 = 0.980$, RMSE = 1.30 °C, $p \ll 0.001$, n = 156. Finally, $U_{38ME}^{K'}$ was regressed to seasonal SSTs following Tierney and Tingley (2018): June-July-August in the North Pacific, August-September-October in the North Atlantic, mean annual SST for all remaining samples. Subsequently, one additional outlying datum was identified using the Rosner test, which was also removed from the calibration dataset. This yields the calibration equation:

$$U_{38ME}^{K'} = SST * 0.034 - 0.036 \tag{6}$$

with $R^2 = 0.972$, RMSE = 1.46 °C, $p \ll 0.001$, and n = 155 (Fig. 3a). All downcore applications of $U_{38ME}^{K'}$ as an SST proxy presented in this paper use equation (6).

3.2. $U_{37}^{K'}$ regression to sea surface temperature

Linear regression of our $U_{37}^{K'}$ data to annual SSTs (Fig. 2b) yields the relationship:

$$U_{37}^{K'} = SST * 0.028 + 0.169 \tag{7}$$

Summary of $U^{K'}$ calibration equations derived in this study. Seasonal refers to the assignment of North Pacific and North Atlantic samples to June-July-August and August-September-October mean sea surface temperature, respectively.

Index	slope	intercept	SST	\mathbb{R}^2	n	RMSE (°C)	Eq. #
$U_{38\mathrm{ME}}^{\mathrm{K'}}$	0.031	0.056	annual	0.964	171	1.84	4
$U_{38ME}^{K^{\prime}}$	0.032	0.016	annual (without sea ice samples)	0.980	156	1.30	5
$U_{38ME}^{K^\prime}$	0.034	-0.036	seasonal	0.972	155	1.46	6
$\mathrm{U}_{37}^{\mathrm{K}'}$	0.028	0.169	annual	0.956	170	2.04	7
$\mathrm{U}_{37}^{\mathrm{K}'}$	0.032	0.081	seasonal	0.974	154	1.37	8
$\mathrm{U}^{\mathrm{K'}}_{\mathrm{38ET}}$	0.024	0.328	annual	0.894	167	3.16	9
$\mathrm{U}^{\mathrm{K'}}_{\mathrm{38ET}}$	0.026	0.257	seasonal	0.919	151	2.97	10

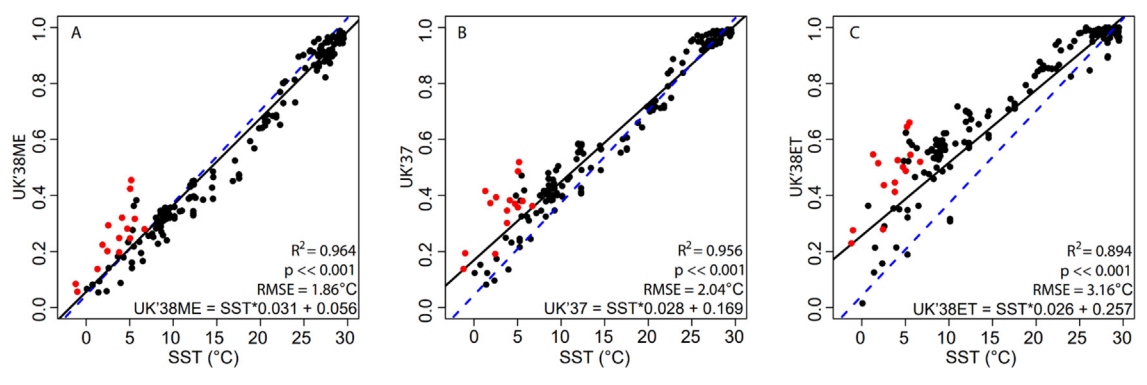


Fig. 2. Calibration of $U_{38}^{K'}$ ratios to annual SST. A. Regression of $U_{38ME}^{K'}$ to annual SST. B. Regression of $U_{37}^{K'}$ to annual SST. C. Regression of $U_{36ME}^{K'}$ to annual SST. D. Regression of $U_{36ME}^{K'}$ to annual SST. Red dots in A and B identify samples in regions affected by sea ice. Blue lines show Müller et al. (1998) calibration for comparison. Note that the $U_{36ME}^{K'}$ measurements were made on the same samples.

J. Novak et al. / Geochimica et Cosmochimica Acta xxx (2022) xxx-xxx

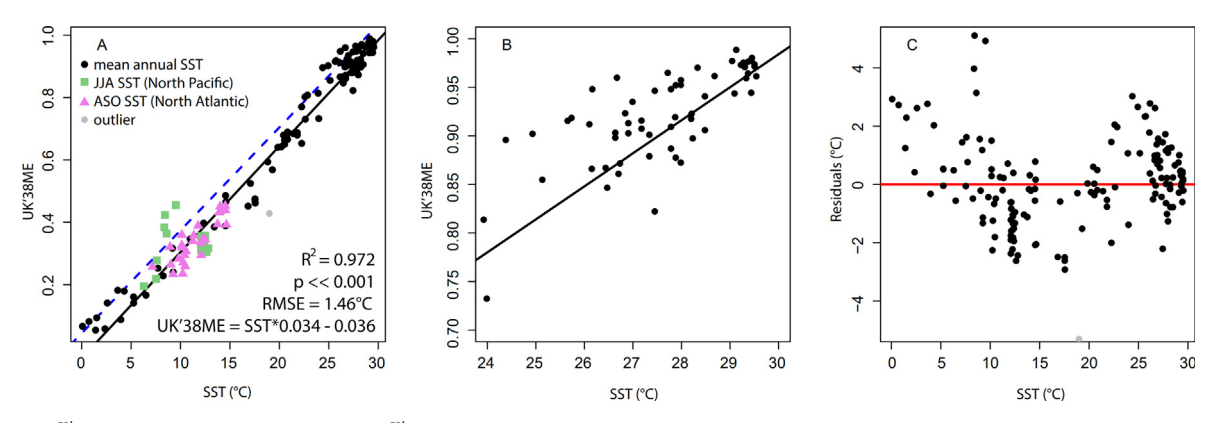


Fig. 3. $U_{38ME}^{K'}$ calibration and residuals. **A.** $U_{38ME}^{K'}$ calibration over 0 to 29.5 °C. North Pacific (green squares) and North Atlantic (purple triangles) were regressed to seasonal SSTs outlined in the text. Remaining data were regressed to mean annual SST (black circles). Blue line shows Müller et al. (1998) calibration for comparison. **B.** Close up of $U_{38ME}^{K'}$ calibration from 24–29.5 °C. C. Difference between the calibrated and observed SST.

with $R^2=0.956$, RMSE = 2.04 °C, $p\ll 0.001$, n=170. Note that n is lower here because $U_{37}^{K'}$ could not be adequately resolved in one sample due to coeluting compounds (Supplementary Table 1). $U_{37}^{K'}$ was then regressed to SST as specified in Tierney and Tingley (2018) and the $U_{37}^{K'}$ datum from the sample identified by the Rosner test as an outlier in the $U_{38ME}^{K'}$ dataset was also removed. This yields the relationship:

$$U_{37}^{K'} = SST * 0.032 + 0.081$$
 (8)
with $R^2 = 0.974$, RMSE = 1.37 °C, $p \ll 0.001$, $n = 154$ (Supplementary Fig. S3).

3.3. Regression of $U_{38ET}^{K'}$ to temperature

Linear regression of our $U_{38ET}^{K'}$ data to annual SSTs (Fig. 2c) yields the relationship:

$$U_{38ET}^{K'} = SST * 0.024 + 0.328 \tag{9}$$

with $R^2=0.894$, RMSE = 3.16 °C, $p\ll 0.001$, n=167 (Supplementary Table 1). Note that n is lower here because $U_{38ET}^{K'}$ could not be adequately resolved in several samples due to coeluting compounds. Linear regression the $U_{38ET}^{K'}$ data to the same seasonal SSTs as $U_{38ME}^{K'}$ and $U_{37}^{K'}$ yields:

$$U_{38ET}^{K'} = SST * 0.026 + 0.257$$
 (10)

with $R^2 = 0.919$, RMSE = 2.47 °C, $p \ll 0.001$, n = 151 (Supplementary Fig. S3).

4. DISCUSSION

4.1. Comparison with previous $U_{38\mathrm{ME}}^{K'}$ calibrations

Our core top derived $U_{38ME}^{K'}$ calibration is similar to previous calibrations of $U_{38ME}^{K'}$ from culture (Conte et al., 1998; Zheng et al., 2019) and suspended particulate organic matter in the upper mixed layer (Conte and Eglinton, 1993). The slopes of the culture (0.037) and suspended organic matter (0.039) calibrations are nearly identical to equation

(6) (0.034), while the intercepts are lower (Fig. 4). Previous studies have attributed disagreements between U₃₇ culture and core top calibrations to a priori different temperature sensitivities among algal strains collected from different ocean basins (Conte et al., 1998; Müller et al., 1998). Chemostat and batch culturing methods may also impose biases on algal temperature sensitivity (Müller et al., 1998; Popp et al., 1998). The $U_{38ME}^{K'}$ culture calibration of Zheng et al. (2019) combines data from experiments with seven E. huxleyi strains and one strain of G. oceanica, which should average out some of the variability introduced by strain-level differences in temperature sensitivity. While the range of temperatures sampled in the Zheng et al. (2019) culture calibration is similar (4–27 °C) to the temperature range represented by our core top dataset (-1) to 29.5 °C), the distribution of samples in SST space differs (Supplementary Fig. S4). Specifically, the culture calibration under-samples growth temperatures below 8 °C relative to our core top dataset (Supplementary Fig. S4), which potentially explains the differences between the culture and core top calibrations.

The often narrow range of SSTs sampled in studies of alkenones in upper mixed layer suspended particulate organic matter has been shown to yield unrealistic $U_{37}^{K'}$ -SST calibrations (Müller et al., 1998). This phenomenon appears responsible for the disagreement between our core top calibration and the upper mixed layer calibration of Conte and Eglinton (1993), which samples a much narrower range of SSTs than our core top dataset (Supplementary Fig. S4). The restricted geographic range of the upper mixed layer alkenone dataset (24°N to 62°N; Conte and Eglinton, 1993) may also play a role.

4.2. High sea surface temperature application

 $U_{38ME}^{K'}$ improves upon the major shortcomings of the $U_{37}^{K'}$ paleothermometer at high temperatures: $U_{38ME}^{K'}$ increases the temperature estimate upper limit and $U_{38ME}^{K'}$ exhibits linearity approaching the upper temperature limit. The $U_{37}^{K'}$ temperature estimate threshold poses major challenges to

J. Novak et al./Geochimica et Cosmochimica Acta xxx (2022) xxx-xxx

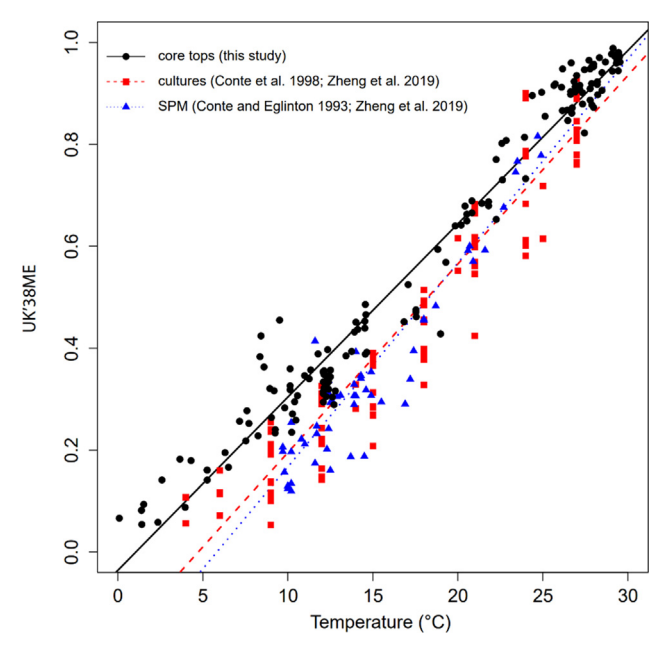


Fig. 4. Core top $U_{38ME}^{K'}$ calibration compared to culture and suspended particulate matter calibrations. Culture data and calibration of Zheng et al. (2019) is shown by the red squares and dashed line. The suspended particulate matter data and calibration of Conte and Eglinton (1993) is shown by the blue triangles and dotted line.

paleoceanographers who seek to study past warm climates, especially tropical regions. For example, $U_{37}^{K'}$ temperature determinations in the Indo-Pacific Warm Pool are essentially invariant in the Pliocene (Pagani et al., 2010; Li et al., 2011). In contrast, TEX₈₆ (O'Brien et al., 2014; Zhang et al., 2014) and foraminiferal Mg/Ca (Wara et al., 2005; O'Brien et al., 2014) proxy records from the Warm Pool in the Pliocene reflect orbital-scale climate variation (albeit with disagreeing absolute temperature estimates) that is not observed in $U_{37}^{K'}$ records (Pagani et al., 2010; Li et al., 2011). This problem persists after reanalysis of $U_{37}^{K'}$ data with BAYSPLINE to generate new SST estimates (Tierney et al., 2019a). Application of BAYSPLINE at high temperatures also carries the potential of amplifying analytical "noise" into signal due to nonlinearity in the calibration (Herbert et al., 2020) since measurement errors lead to an exponential rather than linear departure from the true SST value. Conversely, the widely-applied linear $U_{37}^{K'}$ calibration of Müller et al. (1998) almost certainly underestimates sea surface temperatures as $U_{37}^{K'}$ approaches unity, as evidenced by residuals analysis of alkenone core top data (Conte et al., 2006; Tierney and Tingley, 2018).

Our $U_{38\text{ME}}^{K'}$ calibration (Eq. (6)) yields a saturation temperature (SST when $U_{38\text{ME}}^{K'}=1$) of $\sim 30.4\,^{\circ}\text{C}$ and potentially extends the linear dynamic range of alkenone SST estimates by 7.0 °C relative to the slope attenuation in the BAYS-PLINE $U_{37}^{K'}$ starting at 23.4 °C. Note that the maximum core top SST in our dataset is 29.5 °C, so the 30.4 °C practical temperature estimate threshold is extrapolated from the equation. The higher practical temperature estimate threshold is achieved due to the smaller intercept of the $U_{38\text{ME}}^{K'}$ calibration compared to the Müller et al. (1998)

 $U_{37}^{K'}$ calibration (-0.036 vs. +0.044), so that, at any given temperature, there is more tri-unsaturated relative to diunsaturated $C_{38}ME$ alkenone than the corresponding C_{37} ketones. The slopes of the two equations are almost identical (0.034 vs 0.033; Fig. 3a). $U_{38ME}^{K'}$ residuals from SSTs > 24 °C are normally distributed according to the Shapiro-Wilkes test (p = 0.33) around the mean residual $(0.56 \pm 1.03 \, ^{\circ}\text{C}, \text{Fig. 5})$. While there is a weak but significant relationship between the residuals and SSTs > 24 °C (R = 0.508, p < 0.001, N = 59), the relationship appears to rely on a few highly leveraged datums (N = 5); when they are removed, the relationship between the residuals and SST is insignificant. Together, these tests indicate a linear or only very slightly attenuated slope of the $U_{38ME}^{K'}$ SST calibration over the upper range of SSTs (24-29.5 °C) sampled by our core top sediments, which is vastly improved over $U_{37}^{K'}$

We analyzed a small number of early Pliocene samples from ODP sites 806 and 1143, located in the Western Pacific Warm Pool (Fig. 1, Supplementary Tables 2 and 3), to see whether there is a difference in paleo $U^{K'}_{38ME}$ and $U^{K'}_{37}$ values as they approach saturation. $U^{K'}_{38ME}$ exhibits greater variability than $U^{K'}_{37}$ in the Pliocene samples ($\sigma = 0.014$ vs 0.003) and indicates a greater SST difference between site 806 and 1143, regardless of which $U^{K'}_{37}$ calibration is used (Supplementary Fig. S5). The relationship between $U^{K'}_{38ME}$ and $U^{K'}_{37}$ in the Pliocene samples also matches that seen in the core top samples, suggesting that $U^{K'}_{38ME}$ had a similar linear dynamic range in the early Pliocene as today (Supplementary Fig. S6). At ODP site 1143, $U^{K'}_{38ME}$ generally agrees with BAYSPAR TEX₈₆ and *G. sacculifer Mg/Ca SST*

J. Novak et al./Geochimica et Cosmochimica Acta xxx (2022) xxx-xxx

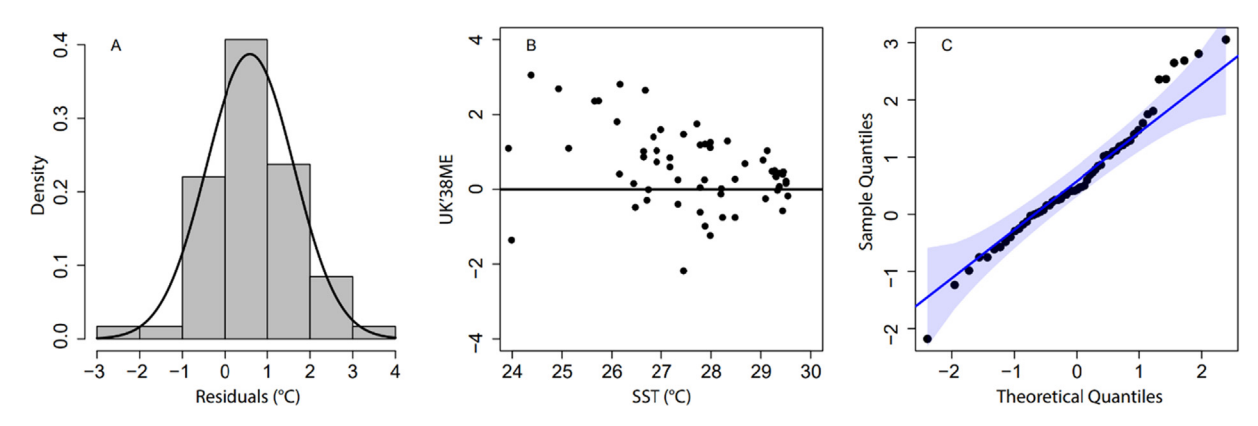


Fig. 5. Analysis of $U_{38ME}^{K'}$ residuals \geq 24 °C. **A** histogram of $U_{38ME}^{K'}$ residuals. **B** $U_{38ME}^{K'}$ residuals relative to SST. **C** q-q plot of normalized $U_{38ME}^{K'}$ residuals data.

estimates (Fig. 6). $U_{38ME}^{K'}$ SST estimates at ODP 1143 and ODP 806 are either warmer or cooler than $U_{37}^{K'}$ SST estimates depending on which $U_{37}^{K'}$ calibration is used (Supplementary Figs. S5, S6). Our $U_{38ME}^{K'}$ data from ODP site 806 is older than published Mg/Ca records (Wara et al., 2005; White and Ravelo, 2020) and available TEX₈₆ data is sparse for our sample interval (Zhang et al., 2014), so comparison to other proxies is not possible. In summary, these data indicate that $U_{38ME}^{K'}$ can reasonably estimate SSTs in Pliocene age sediments where $U_{37}^{K'}$ approaches saturation.

 $U_{38ME}^{K^\prime}$ may, therefore, be particularly useful for study of the Miocene and warm Pliocene, when $U_{37}^{K^\prime}$ saturates in many locations.

4.3. $U_{38ME}^{K'}$: a solution to the species-mixing problem

U_{38ME} is a potential solution to the species-mixing problem encountered in environments with varying sea surface salinity, where Group 3 (e.g. *Emiliania huxleyi*, *Gephyrocapsa oceanica*) and coastal Group 2 haptophytes (e.g. *Isochrysis galbana*, *Ruttnera lamellosa*) cooccur (Salacup

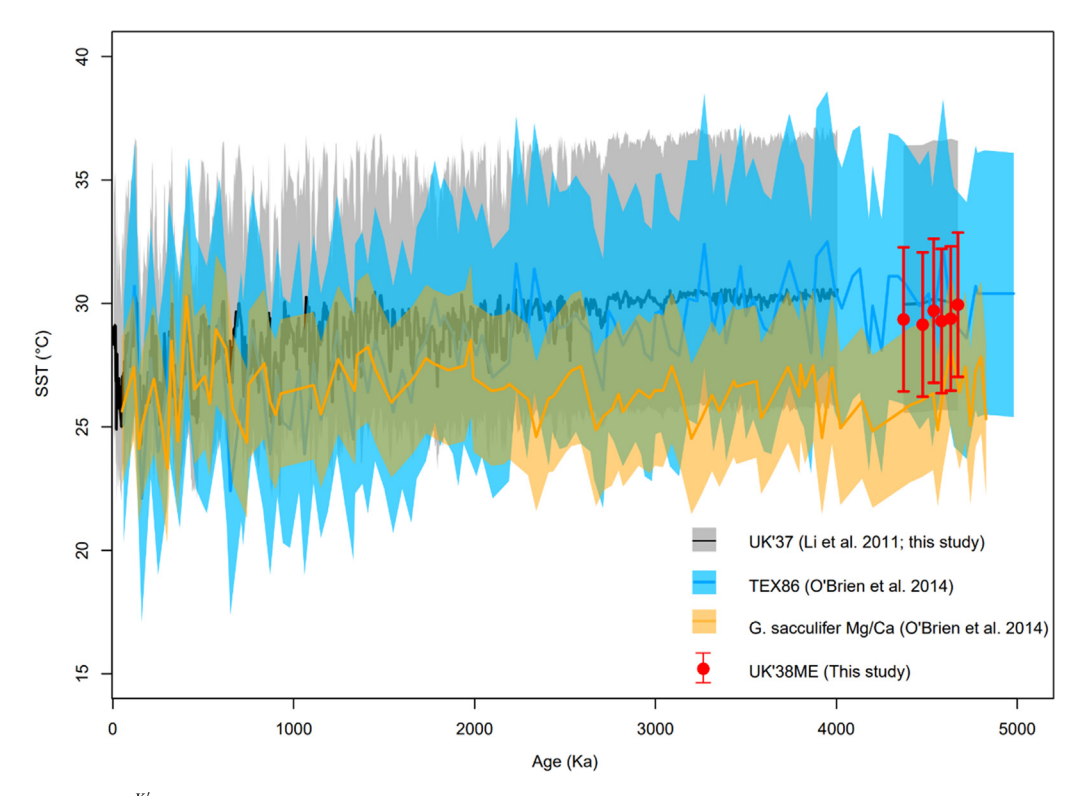


Fig. 6. Comparison of $U_{38ME}^{K'}$ to other SST proxies at ODP 1143. Lines and shading show the median and 95% confidence intervals from the site 1143 $U_{37}^{K'}$ (black), TEX₈₆ (blue), and *G. sacculifer* Mg/Ca (orange) SST records (Li et al., 2011; O'Brien et al., 2014). Red dots and error bars show $U_{38ME}^{K'}$ SST estimates and their 95% confidence interval (this study).

et al., 2019), as $C_{38}ME$ alkenones are either absent or produced only in trace concentrations by Group 2 haptophytes (Zheng et al., 2019). Therefore, we hypothesize that application of $U_{38ME}^{K'}$ in these environments carries less risk of SST estimates biased by production of alkenones by different algal groups.

Recent work on Holocene age sediments from the western basin of the Black Sea (Huang et al., 2021) is an example of the advantage in using $U_{38\text{ME}}^{K'}$ to reconstruct SSTs in environments with multiple alkenone producing Isochrysidales. Group 1, 2, and 3 Isochrysidales have been detected in the Black Sea's sedimentary infill (Huang et al., 2021). Fig. 7 shows $U_{38\text{ME}}^{K'}$ and $U_{37}^{K'}$ data from core GGC18 in the western Black Sea and $U_{37}^{K'}$ data from core GeoTü in the Sea of Marmara, which is connected to the Black Sea by the 30 km long Bosporus Strait (Sperling et al., 2003; Huang et al., 2021; see Fig. 1 for core locations).

The low $\frac{C_{38}ME}{C_{38}ET}$ ratio and high % $C_{37:4}$ between ca. 2450 and 4000 calendar years before present (BP) indicate a per-

iod when the algal community shifted from Group 3 (marine) to Group 2 (brackish) haptophytes (Fig. 7c, d), likely due to a decrease in sea surface salinity caused by changes in the local hydrological balance (Huang et al., 2021). This period is also marked by an apparent increase in SSTs in the western Black Sea that does not occur in the nearby Sea of Marmara (Fig. 7a, b), where salinity is thought to have remained relatively more stable (Sperling et al., 2003). This warming feature in the $U_{37}^{K'}$ record is likely spurious, caused by the shift in the Black Sea algal community rather than an underlying difference in climate between these two proximal sites. The difference in Black Sea SST estimates between $U^{K'}_{38ME}$ and $U^{K'}_{37}$ averages 5.51 $^{\circ}C$ $(U^{K'}_{37}$ warmer) between 2450 and 4000 years BP compared to 0.23 °C in the rest of the core. The $U^{K'}_{38ME}\mbox{-inferred SSTs}$ between 2450 and 4000 years BP better agree with the SST data from the Sea of Marmara (Fig. 7a, b), albeit imperfectly. This may be due to a greater contribution of Group 2 Isochrysidales to sedimentary C₃₈ME alkenone concentrations as the $\frac{C_{38}ME}{C_{38}ET}$ ratio approaches 0 (average

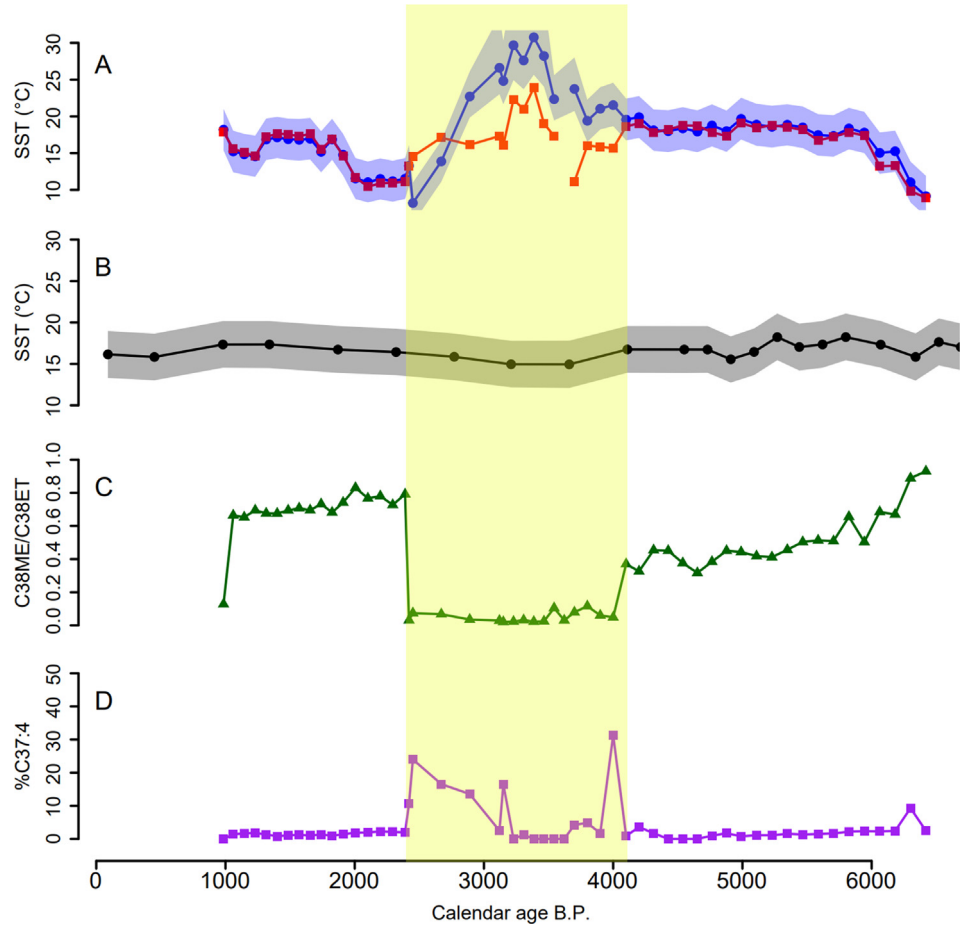


Fig. 7. Application of $U_{38ME}^{K'}$ to Holocene age sediments from the Black Sea. **A.** $U_{38ME}^{K'}$ (red squares) and $U_{37}^{K'}$ (blue circles) BAYSPLINE-generated SST estimates from core GGC18 in the western Black Sea. **B.** $U_{37}^{K'}$ BAYSPLINE-generated SST estimates from core GeoTü in the Sea of Marmara. **C.** $\frac{C_{38}ME}{C_{38}ET}$ alkenone ratio in the Black Sea samples. **D.** %C_{37:4} in the Black Sea samples. Yellow box shoes the period of inferred algal community shift from Group III (marine) to Group II (brackish) Isochrysidales. Grey and blue shading shows the 95% confidence interval for $U_{37}^{K'}$ BAYSPLINE-generated SSTs.

value in our core tops = 0.572), which is supported by a weak but statistically significant negative relationship between the $\frac{C_{38}ME}{C_{38}ET}$ ratio and $U_{38ME}^{K'}$ -inferred SSTs between 2450 and 4000 years BP (Spearman's ρ = -0.57, p = 0.035). It is also possible that the increased abundance of Group 2 Isochrysidales prompted a shift in the bloom season of *E. huxleyi*, potentially skewing SST estimates towards warmer months. Black Sea summer SSTs average ~23–24 °C, approximating $U_{38ME}^{K'}$ -inferred SSTs in the 2450 and 4000 years BP interval (Shaltout and Omstedt, 2014). Changes in riverine and precipitation inputs to surface waters may have also produced complicated SST patterns in the Black Sea. Regardless, $U_{38ME}^{K'}$ SSTs are more congruent with the Sea of Marmara record than $U_{37}^{K'}$ data from the Black Sea.

4.4. Influence of seasonal production on $U_{38ME}^{K'}$

Core top studies have shown systematically warm $U_{27}^{K'}$ residuals in both the North Pacific and North Atlantic that are attributed to seasonally skewed primary productivity (Prahl et al., 2010; Filipova et al., 2016; Max et al., 2020). These regional seasonality effects were summarized in the BAYSPLINE global U₃₇^{K'} calibration effort as recording June-July-August SST in the North Pacific and August-September-October SST in the North Atlantic (Tierney and Tingley, 2018). In the open ocean, C₃₇ and C_{38ME} alkenones are produced exclusively by the same organisms: Emiliania huxleyi and Gephyrocapsa oceanica (Volkman et al., 1980, 1995; Zheng et al., 2019). So, it is expected that seasonal production of alkenones, as documented in the North Pacific and North Atlantic ocean regions by sediment traps (Harada et al., 2006; Seki et al., 2007; Rosell-Melé and Prahl, 2013), imparts a comparable seasonal SST estimate bias onto $U_{37}^{K'}$ and $U_{38ME}^{K'}$.

To test this expectation, the residuals of core top $U_{38ME}^{K'}$ -derived SST estimates to annual SSTs and the seasonal SSTs outlined above were compared (Fig. 8), which yielded no obvious conclusions as to how production seasonality

affects sedimentary $U_{38ME}^{K'}$ values in the North Pacific and North Atlantic. The mean residual from the seasonal regression (Eq. (6)) was smaller than the annual regression (Eq. (5)) in both the North Pacific (1.55 vs. -0.37 °C, Welch's one-sided t-test, $p \ll 0.001$, df = 36.8) and North Atlantic (1.41 vs -0.45 °C, Welch's one-sided t-test, $p \ll 0.001$, df = 51) samples. The variance of the residuals from the annual regression was smaller than the variance of the seasonal regression residuals in the North Pacific (p = 0.006, df = 23, one-sided F-test), while there was no statistically significant difference in the North Atlantic. For the seasonal regression, residuals from the North Pacific show notable positive ($\widetilde{\mu}_3 = 1.25$) skewness, while North Pacific residuals from the mean annual regression show weaker negative ($\widetilde{\mu}_3 = -0.73$) skewness (Fig. 8).

It is likely that overrepresentation of the North Pacific and North Atlantic regions in our dataset (ca. 41% of samples) hinders more effective investigation of production seasonality on sedimentary $U_{38ME}^{K'}$ in these regions due to the strong influence of these data on the regression coefficients. Inclusion of high latitude core tops from the southern hemisphere (ca. 12% of samples) may further confound this analysis due to a summer seasonal bias in core top $U_{37}^{K'}$ values found by some regional studies (Sikes et al., 1997). Around New Zealand, sediment trap study of $U_{37}^{K'}$ has shown a significant seasonality to alkenone export (Sikes et al., 2005; Rigual-Hernández et al., 2021) that is evident in downcore comparisons of $U_{37}^{K'}$ to other SST proxies (Sikes et al., 2019). Similarly, recent core top study of *Glo*bigerinoides ruber δ¹⁸O and Mg/Ca values along the northwest Australian Margin indicates an SST estimate bias towards warmer austral fall temperatures (Pei et al., 2021) that may also affect alkenone distributions in the southernmost samples of our core top transect there (n = 2). However, there is no widely-observed seasonality effect on sedimentary $U_{37}^{K'}$ values in the cold Southern Ocean in the data compilation of the recent BAYSPLINE calibration (Tierney and Tingley, 2018). Residuals analysis of the Southern Ocean $U_{38ME}^{K'}$ core top data does not show a clear

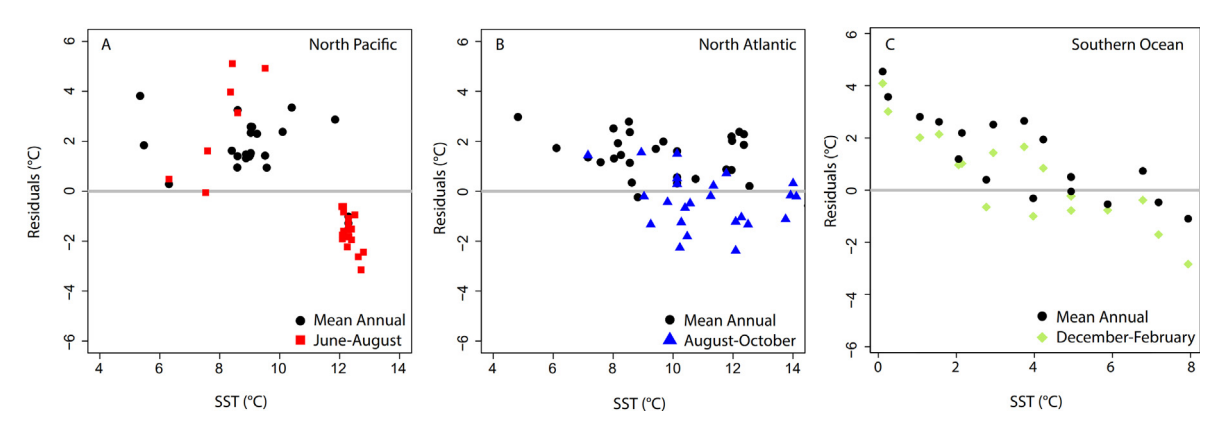


Fig. 8. Residuals analysis of annual (Eq. (5)) and seasonal (Eq. (6)) regressions of $U_{38ME}^{K'}$ to sediments from the North Pacific, North Atlantic, and Southern Ocean. (A) North Pacific residuals. (B) North Atlantic residuals. (C) Southern Ocean residuals.

seasonal residuals trend either (Fig. 8) and there is no statistically significant difference between the mean residual or variance when regressing to mean annual versus summer SSTs. While we do see a significant relationship between residuals in the Southern Ocean and SST (R=0.834, p<0.001), this only strengthens when regressing to summer SSTs (R=0.879, p<0.001) rather than mean annual SST. This relationship may indicate some slope attenuation at the low-end of the calibration temperature range, as has been suspected previously in core top study of $U_{37}^{K'}$ (Tierney and Tingley, 2018).

Although the test statistics of the annual regression (Eq. (5)) are slightly stronger, the seasonal regression (Eq. (6)) was used for the downcore applications of $U_{38\text{ME}}^{K'}$ shown above for three reasons: (1) logically, $U_{38\text{ME}}^{K'}$ should be regressed to SSTs from the season of greatest alkenone flux to the sediments; (2) calibration to mean annual temperature is likely only possible in regions where the mean coincides with the SST range of haptophyte growth season; (3) the downcore SST estimates from the seasonal regression are most congruent with BAYSPLINE-generated $U_{37}^{K'}$ SST paleodeterminations.

4.5. The $U_{38FT}^{K'}$ paleothermometer

Despite the relatively high abundance of di-unsaturated $C_{38}ET$ alkenone at lower SSTs, $U_{38ET}^{K'}$ does not appear to be well-suited for estimating SSTs in polar regions due to the scatter in the $U_{38FT}^{K'}$ -SST relationship below 5 °C observed in our data, which is reflected by the high RMSE value (3.17 °C; Fig. 2c). Unlike the $U_{37}^{K'}$ and $U_{38ME}^{K'}$ data, there are both large positive and negative outliers in the $U_{38{\rm ET}}^{K'}$ dataset. While calibration of $U_{38ET}^{K'}$ to seasonal SSTs improves the correlation coefficient somewhat (Supplementary Fig. S3), the large negative residuals remain (Supplementary Fig. S7). These large negative residuals appear to be an artifact generated by the much higher intercept of the $U_{38ET}^{K'}$ -SST calibration than the other $U^{K'}$ indices measured in this study (Table 1), where the large intercept incorrectly describes the relationship between $U_{38FT}^{K'}$ and temperature below ~5 °C. Other regression models (e.g., power law, polynomial) generate similarly unsatisfying residuals patterns (not shown). Until the source of the scatter in the $U_{38\text{ET}}^{K'}\text{-SST}$ relationship is identified and resolved, it is recommended that $U_{38ET}^{K'}$ not be used as a paleothermometer.

5. CONCLUSIONS

We measured $U_{37}^{K'}$ and $U_{38ME}^{K'}$ in a globally distributed set of marine core top sediments. Our data demonstrate that a previously disregarded alkenone paleothermometer, $U_{38ME}^{K'}$, offers an alternative linear proxy to $U_{37}^{K'}$ when estimating SSTs up to at least 29.5 °C, the warmest SST observed in our surface sediment sample set. We measured $U_{38ME}^{K'}$ and $U_{37}^{K'}$ in early Pliocene age sediments from the Indo-Pacific

Warm Pool, which demonstrated that $U_{38ME}^{K'}$ exhibits greater variability than $U_{37}^{K'}$ as the indices approach saturation ($U^{K'} \rightarrow 1$). Our Pliocene $U^{K'}_{38ME}$ data from ODP 1143 agree with published TEX86 and G. sacculifer Mg/Ca SST estimates from the same core. Extension of the alkenone SST estimate range holds great potential for resolving outstanding questions about SST patterns in past warm climates of the Pliocene and Miocene. $U_{37}^{K'}$ SST estimates in the Indo-Pacific Warm Pool are essentially invariant in the Pliocene (Fig. 6), unlike TEX₈₆ and Mg/Ca-based estimates (Wara et al., 2005; Li et al., 2011; O'Brien et al., 2014), and the magnitude of the estimated SSTs are essentially determined by the individual's choice of $U_{37}^{K^\prime}$ calibration, cf. (Müller et al., 1998; Zhang et al., 2014; Tierney and Tingley, 2018; Tierney et al., 2019a). $U_{38ME}^{K'}$'s greater linear dynamic range gives paleoceanographers a foothold to estimate SSTs in warm climate conditions (using equation (6)). Since $U^{K'}_{\rm 38ME}$ and $U^{K'}_{\rm 37}$ are measured simultaneously in samples, they can also be used together to generate higherconfidence SST estimates in sediments where both are unsaturated, providing a check on each other in samples with complex chromatographic backgrounds. However, it should be noted that $U_{38ME}^{K'}$ measurements in our core top samples required more intensive sample preparation than typical U₃₇ analyses, indicating a potential shortfall of the proxy using the current analytical method.

We also propose $U_{38ME}^{K'}$ as a generally applicable solution to the challenge of producing reliable SST records from sediments in brackish estuarine and closed-basin environments where Group III (marine) and Group II (brackish) haptophytes cohabitated. We demonstrate the superior performance of $U_{38ME}^{K'}$ over $U_{37}^{K'}$ in brackish environments by application of both proxies to a published Holocene-age alkenone record from the Black Sea by comparison to a record from the Sea of Marmara. We show that $U_{38ME}^{K'}$ produces reasonable SST estimates while $U_{37}^{K'}$ generates implausibly warm SSTs in the same samples where there is likely mixing of alkenones produced by Group III and Group II haptophytes.

Declaration of Competing Interest

The authors declare that they have no known competing financial interests or personal relationships that could have appeared to influence the work reported in this paper.

ACKNOWLEDGMENTS

The authors thank Woods Hole Oceanographic Institute, Lamont-Doherty Earth Observatory, Oregon State University, GEOMAR-Helmholtz Centre for Ocean Research, the Scripps Institute of Oceanography and their sediment repository curators, Dr. Ann Holbourn and the shipboard scientific party of of R/V Sonne cruise SO257, Dr. Beth Caissie and the shipboard scientific party of the Amundson cruise for providing us with samples for this study. The authors thank Dr. Timothy D. Herbert for feed-

back on early manuscript drafts. The authors are grateful for the thorough and extensive comments from the associate editor, Dr. Jessica Tierney, which greatly improved the manuscript. This research is funded by NSF EAR-1762431 to Yongsong Huang. Funding for the R/V Sonne cruise SO257 was provided by the German Federal Ministry of Education and Research (Grant SO-257, WACHEIO, 03G0257A). All data is archived at PAN-GAEA: https://doi.pangaea.de/10.1594/PANGAEA. 942968.

AUTHOR CONTRIBUTIONS

Y.H. initiated the research idea and funded the project. Y.H., S.M.M., and J.N. designed the study and wrote the draft. J.N., K.J.W., and S.L. performed the alkenone analyses. S.M.M. compiled the modern SST data. J.N. conducted the data analysis. All authors contributed to interpreting the data and improving the manuscript.

APPENDIX A. SUPPLEMENTARY MATERIAL

Supplementary data to this article can be found online at https://doi.org/10.1016/j.gca.2022.04.021.

REFERENCES

- Anand P., Elderfield H. and Conte M. H. (2003) Calibration of Mg/Ca thermometry in planktonic foraminifera from a sediment trap time series. *Paleoceanography* 18.
- Ausín B., Haghipour N., Bruni E. and Eglinton T. (2021) The influence of lateral transport on sedimentary alkenone paleoproxy signals. *Biogeosci. Discuss.* 1–25.
- Banzon V., Smith T. M., Liu C. and Hankins W. (2016) A long-term record of blended satellite and in situ sea surface temperature for climate monitoring, modeling and environmental studies. Earth Syst. Sci. Data Discuss. 1–13.
- Bendle J. and Rosell-Melé A. (2004) Distributions of UK37 and UK'37 in the surface waters and sediments of the Nordic Seas: Implications for paleoceanography. *Geochem. Geophys. Geosyst.* 5, 1–19.
- Bendle J. A. P., Rosell-Melé A., Cox N. J. and Shennan I. (2009) Alkenones, alkenoates, and organic matter in coastal environments of NW Scotland: Assessment of potential application for sea level. *Geochem. Geophys. Geosyst.* 10.
- Bentaleb I., Fontugne M. and Beaufort L. (2002) Long-chain alkenones and Uk'37 variability along a south-north transect in the Western Pacific Ocean. *Glob Planet Change* **34**, 173–183.
- Chaisson W. P. and Leckie R. M. (1993) High-resolution Neogene planktonic foraminifer biostratigraphy of Site 806, Ontong Java Plateau (western equatorial Pacific). In *Proc, Sci results, ODP, Leg 130, Ontong Java Plateau*, pp. 137–178.
- Conte M. H. and Eglinton G. (1993) Alkenone and alkenoate distributions within the euphotic zone of the eastern North Atlantic: correlation with production temperature. *Deep Res.* Part I 40, 1935–1961.
- Conte M. H., Sicre M. A. and Rühlemann C., et al. (2006) Global temperature calibration of the alkenone unsaturation index (UK'37) in surface waters and comparison with surface sediments. *Geochem. Geophys. Geosyst.* 7.
- Conte M. H., Thompson A. and Eglinton G. (1994) Primary production of lipid biomarker compounds by Emiliania hux-

- leyi. Results from an experimental mesocosm study in fjords of southwestern Norway. *Sarsia* **79**, 319–331.
- Conte M. H., Thompson A., Lesley D. and Harris R. P. (1998) Genetic and physiological influences on the alkenone/alkenoate versus growth temperature relationship in Emiliania huxleyi and Gephyrocapsa oceanica. *Geochim. Cosmochim. Acta* **62**, 51–68.
- Conte M. H., Weber J. C., King L. L. and Wakeham S. G. (2001) The alkelone temperature signal in Western North Atlantic surface waters. *Geochim. Cosmochim. Acta* 65, 4275–4287.
- D'Andrea W. J., Liu Z. and Alexandre M. D. R., et al. (2007) An efficient method for isolating individual long-chain alkenones for compound-specific hydrogen isotope analysis. *Anal. Chem.* **79**, 3430–3435.
- Dekens P. S., Lea D. W., Pak D. K. and Spero H. J. (2002) Core top calibration of Mg/Ca in tropical foraminifera: Refining paleotemperature estimation. *Geochem. Geophys. Geosyst.* 3, 1–29.
- Dillon J. T. and Huang Y. (2015) TEXPRESS v1.0: A MATLAB toolbox for efficient processing of GDGT LC-MS data. *Org. Geochem.* **79**, 44–48.
- Dillon J. T., Longo W. M. and Zhang Y., et al. (2016) Identification of double-bond positions in isomeric alkenones from a lacustrine haptophyte. *Rapid Commun. Mass Spectrom.* 30, 112–118.
- Divine D. V. and Dick C. (2006) Historical variability of sea ice edge position in the Nordic Seas. *J. Geophys. Res. Ocean* 111, 1–14
- Elderfield H. and Ganssen G. (2000) Past temperature and δ^{18} O of surface ocean waters inferred from foraminiferal Mg/Ca ratios. *Nature* **405**, 442–445.
- Epstein B. L., D'Hondt S. and Quinn J. G., et al. (1998) An effect of dissolved nutrient concentrations on alkenone-based temperature estimates. *Paleoceanography* 13, 122–126.
- Epstein S., Ruchsbaum R., Lowenstam H. A. and Urey H. C. (1953) Revised Carbonate-Water Isotopic Temperature Scale. *Bull. Geol. Soc. Am.* 64, 1315–1326.
- Erez J. and Luz B. (1983) Experimental paleotemperature equation for planktonic foraminifera. *Geochim. Cosmochim. Acta* 47, 1025–1031.
- Filipova A., Kienast M., Frank M. and Schneider R. R. (2016) Alkenone paleothermometry in the North Atlantic: A review and synthesis of surface sediment data and calibrations. *Geochem. Geophys. Geosyst.* 17, 1312–1338.
- Goni M. A., Hartz D. M., Thunell R. C. and Tappa E. (2001) Oceanographic considerations for the application of the alkenone-based paleotemperature UK'37 index in the Gulf of California. *Geochim. Cosmochim. Acta* 65, 545–557.
- Gould J., Kienast M. and Dowd M. (2017) Investigation of the UK'37 vs. SST relationship for Atlantic Ocean suspended particulate alkenones: An alternative regression model and discussion of possible sampling bias. *Deep Res. Part I Oceanogr. Res. Pap.* 123, 13–21.
- Harada N., Sato M., Shiraishi A. and Honda M. C. (2006) Characteristics of alkenone distributions in suspended and sinking particles in the northwestern North Pacific. *Geochim. Cosmochim. Acta* 70, 2045–2062.
- Herbert T. D. (2001) Review of alkenone calibrations (culture, water column, and sediments). *Geochem. Geophys. Geosyst.* 2.
- Herbert T. D. (2003) Alkenone Paleotemperature Determinations. Treatise on. *Geochemistry* 6–9, 391–432.
- Herbert T. D., Rose R. and Dybkjær K., et al. (2020) Bihemispheric Warming in the Miocene Climatic Optimum as Seen From the Danish North Sea. *Paleoceanogr. Paleoclimatol.* **35**, 1–10.

- Hernández-Sánchez M. T., Woodward E. M. S. and Taylor K. W. R., et al. (2014) Variations in GDGT distributions through the water column in the South East Atlantic Ocean. *Geochim. Cosmochim. Acta* 132, 337–348.
- Huang Y., Zheng Y. and Heng P., et al. (2021) Black Sea paleosalinity evolution since the last deglaciation reconstructed from alkenone-inferred Isochrysidales diversity. *Earth Planet. Sci. Lett.* **564** 116881.
- Imbrie J. and Kipp N. G. (1971) A new micropaleontological method for quantitative paleoclimatology: application to a late Pleistocene Caribbean core. In *The late Cenozoic glacial ages* (ed. K. Turekian). Yale University Press, New Haven, pp. 71– 181.
- Jahnke R. A. and Knight L. H. (1997) A gravity-driven, hydraulically-damped multiple piston corer for sampling fine-grained sediments. *Deep Res. Part I Oceanogr. Res. Pap.* 44, 713–718.
- Kaiser J., Wang K. J. and Rott D., et al. (2019) Changes in long chain alkenone distributions and Isochrysidales groups along the Baltic Sea salinity gradient. Org. Geochem. 127, 92–103.
- Karner M. B., Delong E. F. and Karl D. M. (2001) Archaeal dominance in the mesopelagic zone of the Pacific Ocean. *Nature* 409, 507–510.
- Kucera M., Weinelt M. and Kiefer T., et al. (2005) Reconstruction of sea-surface temperatures from assemblages of planktonic foraminifera: Multi-technique approach based on geographically constrained calibration data sets and its application to glacial Atlantic and Pacific Oceans. Quat. Sci. Rev. 24, 951–998.
- Lawrence K. T., Pearson A. and Castañeda I. S., et al. (2020) Comparison of Late Neogene U k' 37 and TEX 86 Paleotemperature Records from the Eastern Equatorial Pacific at Orbital Resolution. *Paleoceanogr. Paleoclimatol.* 35, 1–16.
- Li L., Li Q. and Tian J., et al. (2011) A 4-Ma record of thermal evolution in the tropical western Pacific and its implications on climate change. *Earth Planet. Sci. Lett.* **309**, 10–20.
- Longo W. M., Dillon J. T. and Tarozo R., et al. (2013) Unprecedented separation of long chain alkenones from gas chromatography with a poly(trifluoropropylmethylsiloxane) stationary phase. *Org. Geochem.* **65**, 94–102.
- Malevich S. B., Vetter L. and Tierney J. E. (2019) Global Core Top Calibration of δ¹⁸O in Planktic Foraminifera to Sea Surface Temperature. *Paleoceanogr. Paleoclimatol.* 34, 1292–1315.
- Martínez-Sosa P., Tierney J. E. and Stefanescu I. C., et al. (2021) A global Bayesian temperature calibration for lacustrine brGDGTs. Geochim. Cosmochim. Acta 305, 87–105.
- Massey F. J. (1951) The Kolmogorov-Smirnov Test for Goodness of Fit. J. Am. Stat. Assoc. 46, 68–78.
- Max L., Lembke-Jene L. and Zou J., et al. (2020) Evaluation of reconstructed sea surface temperatures based on U^{k'}₃₇ from sediment surface samples of the North Pacific. *Quat. Sci. Rev.* 243 106496.
- Meier W. N., Fetterer F. and Savoie M., et al. (2017) NOAAI NSIDC Climate Data Record of Passive Microwave Sea Ice Concentration, Version 3. [1980-2010].
- Mercer J. L., Zhao M. and Colman S. M. (2005) Seasonal variations of alkenones and UK37 in the Chesapeake Bay water column. *Estuar. Coast. Shelf Sci.* 63, 675–682.
- Millard S. P. and Kowarik A. (2018) Package 'EnvStats'.
- Müller P. J., Kirst G. and Ruhland G., et al. (1998) Calibration of the alkenone paleotemperature index UK'37 based on core-tops from the eastern South Atlantic and the global ocean (60°N-60° S). *Geochim. Cosmochim. Acta* **62**, 1757–1772.
- Mysak L. A. and Manak D. K. (1989) Arctic sea-ice extent and anomalies, 1953–1984. *Atmos. Ocean* 27, 376–405.
- Nürnberg D., Bijma J. and Hemleben C. (1996) Assessing the reliability of magnesium in foraminiferal calcite as a proxy for

- water mass temperatures. *Geochim. Cosmochim. Acta* **60**, 803–814.
- O'Brien C. L., Foster G. L. and Martínez-Botí M. A., et al. (2014) High sea surface temperatures in tropical warm pools during the Pliocene. *Nat. Geosci.* 7, 606–611.
- Pagani M., Liu Z., Lariviere J. and Ravelo A. C. (2010) High Earth-system climate sensitivity determined from Pliocene carbon dioxide concentrations. *Nat. Geosci.* 3, 27–30.
- Parkinson C. L. and Gratz A. J. (1983) On the seasonal sea ice cover of the Sea of Okhotsk. J. Geophys. Res. Oceans 88, 2793– 2802
- Pei R., Kuhnt W. and Holbourn A., et al. (2021) Evolution of Sea Surface Hydrology Along the Western Australian Margin Over the Past 450 kyr. *Paleoceanogr. Paleoclimatol.* **36**, 1–19.
- Peng G., Meier W. N., Scott D. J. and Savoie M. H. (2013) A long-term and reproducible passive microwave sea ice concentration data record for climate studies and monitoring. *Earth Syst. Sci. Data* 5, 311–318.
- Popp B. N., Kenig F. and Wakeham S. G., et al. (1998) Does growth rate affect ketone unsaturation and intracellular carbon isotopic variability in Emiliania huxleyi? *Paleoceanography* 13, 35–41.
- Prahl F. G., Muehlhausen L. A. and Zahnle D. L. (1988) Further evaluation of long-chain alkenones as indicators of paleoceanographic conditions. *Geochim. Cosmochim. Acta* 52, 2303–2310.
- Prahl F. G., Rontani J. F. and Zabeti N., et al. (2010) Systematic pattern in U₃^{K'} Temperature residuals for surface sediments from high latitude and other oceanographic settings. *Geochim. Cosmochim. Acta* 74, 131–143.
- Prahl F. G. and Wakeham S. G. (1987) Calibration of unsaturation patterns in long-chain ketone compositions for palaeotemperature assessment. *Nature* 330, 367–369.
- Prahl F. G., Wolfe G. V. and Sparrow M. A. (2003) Physiological impacts on alkenone paleothermometry. *Paleoceanography* **18**, 1–7
- Richey J. N. and Tierney J. E. (2016) GDGT and alkenone flux in the northern Gulf of Mexico: Implications for the TEX86 and UK'37 paleothermometers. *Paleoceanography* **31**, 1547–1561.
- Richter N., Russell J., Garfinkel J. and Huang Y. (2020) Cold season warming in the North Atlantic during the last 2000 years: Evidence from Southwest Iceland. Clim. Past Discuss. 1– 28
- Rigual-Hernández A. S., Sierro F. J. and Flores J. A., et al. (2021) Influence of environmental variability and Emiliania huxleyi ecotypes on alkenone-derived temperature reconstructions in the subantarctic Southern Ocean. *Sci. Total Environ.* 812, 152474.
- Rosell-Melé A., Eglinton G., Pflaumann U. and Sarnthein M. (1995) Atlantic core-top calibration of the UK37 index as a seasurface palaeotemperature indicator. *Geochim. Cosmochim. Acta* 59, 3099–3107.
- Rosell-Melé A. and Prahl F. G. (2013) Seasonality of UK'37 temperature estimates as inferred from sediment trap data. *Quat. Sci. Rev.* 72, 128–136.
- Rosner B. (1983) Percentage points for a generalized esd manyoutlier procedure. *Technometrics* **25**, 165–172.
- Russell A. D., Hönisch B., Spero H. J. and Lea D. W. (2004) Effects of seawater carbonate ion concentration and temperature on shell U, Mg, and Sr in cultured planktonic foraminifera. *Geochim. Cosmochim. Acta* 68, 4347–4361.
- Salacup J. M., Farmer J. R., Herbert T. D. and Prell W. L. (2019) Alkenone Paleothermometry in Coastal Settings: Evaluating the Potential for Highly Resolved Time Series of Sea Surface Temperature. *Paleoceanogr. Paleoclimatol.* 34, 164–181.
- Sawada K., Handa N. and Shiraiwa Y., et al. (1996) Long-chain alkenones and alkyl alkenoates in the coastal and pelagic

- sediments of the northwest north Pacific, with special reference to the reconstruction of Emiliania huxleyi and Gephyrocapsa oceanica ratios. *Org. Geochem.* **24**, 751–764.
- Schouten S., Hopmans E. C., Schefuß E. and Sinninghe Damsté J. S. (2002) Distributional variations in marine crenarchaeotal membrane lipids: a new tool for reconstructing ancient sea water temperatures? *Earth Planet. Sci. Lett.* 204, 265–274.
- Seki O., Nakatsuka T. and Kawamura K., et al. (2007) Time-series sediment trap record of alkenones from the western Sea of Okhotsk. Mar. Chem. 104, 253–265.
- Shackleton N. J. (1987) Oxygen Isotopes, Ice Volume and Sea Level. *Ouat. Sci.* **6**, 183–190.
- Shaltout M. and Omstedt A. (2014) Recent sea surface temperature trends and future scenarios for the Mediterranean Sea. *Oceanologia* **56**, 411–443.
- Shapiro S. S. and Wilk M. B. (1965) An Analysis of Variance Test for Normality (Complete Samples). *Biometrika* **52**, 591.
- Sicre M.-A., Bard E., Ezat U. and Rostek F. (2002) Alkenone distributions in the North Atlantic and Nordic sea surface waters. Geochem. Geophys. Geosyst., 3:1 of 13–13 13.
- Sikes E. L., Farrington J. W. and Keigwin L. D. (1991) Use of the alkenone unsaturation ratio UK37 to determine past sea surface temperatures: core-top SST calibrations and methodology considerations. *Earth Planet. Sci. Lett.* 104, 36–47.
- Sikes E. L., O'Leary T., Nodder S. D. and Volkman J. K. (2005) Alkenone temperature records and biomarker flux at the subtropical front on the chatham rise, SW Pacific Ocean. *Deep Res. Part I Oceanogr. Res. Pap.* 52, 721–748.
- Sikes E. L., Schiraldi B. and Williams A. (2019) Seasonal and Latitudinal Response of New Zealand Sea Surface Temperature to Warming Climate Since the Last Glaciation: Comparing Alkenones to Mg/Ca Foraminiferal Reconstructions. *Paleoceanogr. Paleoclimatol.* 34, 1816–1832.
- Sikes E. L. and Volkman J. K. (1993) Calibration of alkenone unsaturation ratios (UK'37) for paleotemperature estimation in cold polar waters. *Geochim. Cosmochim. Acta* 57, 1883–1889.
- Sikes E. L., Volkman J. K., Robertson L. G. and Pichon J. J. (1997) Alkenones and alkenes in surface waters and sediments of the Southern Ocean: Implications for paleotemperature estimation in polar regions. *Geochim. Cosmochim. Acta* 61, 1495–1505.
- Smith W. O. and Comiso J. C. (2008) Influence of sea ice on primary production in the Southern Ocean: A satellite perspective. J. Geophys. Res. Ocean 113, 1–19.
- Sonzogni C., Bard E. and Rostek F., et al. (1997) Core-top calibration of the alkenone index vs sea surface temperature in the Indian Ocean. *Deep Res. Part II Top Stud. Oceanogr.* 44, 1445–1460.
- Sperling M., Schmiedl G. and Hemleben C., et al. (2003) Black Sea impact on the formation of eastern Mediterranean sapropel S1?
 Evidence from the Marmara Sea. *Palaeogeogr. Palaeoclimatol. Palaeoecol.* 190, 9–21.
- Spero H. J., Bijma J., Lea D. W. and Bernis B. E. (1997) Effect of seawater carbonate concentration on foraminiferal carbon and oxygen isotopes. *Nature* 390, 497–500.
- Telford R. J., Li C. and Kucera M. (2013) Mismatch between the depth habitat of planktonic foraminifera and the calibration depth of SST transfer functions may bias reconstructions. *Clim. Past* **9**, 859–870.
- Ternois Y., Sicre M. A. and Boireau A., et al. (1997) Evaluation of long-chain nikenones as paleo-temperature indicators in the mediterranean sea. *Deep Res. Part I Oceanogr. Res. Pap.* 44, 271–286.

- Tian J., Wang P., Cheng X. and Li Q. (2002) Astronomically tuned Plio-Pleistocene benthic δ^{18} O record from South China Sea and Atlantic-Pacific comparison. *Earth Planet. Sci. Lett.* **203**, 1015–1029
- Tierney J. E., Haywood A. M. and Feng R., et al. (2019a) Pliocene Warmth Consistent With Greenhouse Gas Forcing. *Geophys. Res. Lett.* **46**, 9136–9144.
- Tierney J. E., Malevich S. B. and Gray W., et al. (2019b) Bayesian Calibration of the Mg/Ca Paleothermometer in Planktic Foraminifera. *Paleoceanogr. Paleoclimatol.* **34**, 2005–2030.
- Tierney J. E. and Tingley M. P. (2018) BAYSPLINE: A New Calibration for the Alkenone Paleothermometer. *Paleoceanogr. Paleoclimatol.* 33, 281–301.
- Tierney J. E. and Tingley M. P. (2014) A Bayesian, spatially-varying calibration model for the TEX86 proxy. Geochim. Cosmochim. Acta 127, 83–106.
- Tuit C. B. and Wait A. D. (2020) A review of marine sediment sampling methods. *Environ. Forensics* **21**, 291–309.
- Urey H. C. (1947) The thermodynamic properties of isotopic substances. Liversidge lecture, delivered before the Chemical Society in the Royal Institution on December 18th, 1946. *J. Chem. Soc.*, 562–581.
- Volkman J. K., Barrett S. M., Blackburn S. I. and Sikes E. L. (1995) Gephyrocapsa oceanica: Implications for the studies of paleoclimate. *Geochem. Cosmochim. Acta* 59, 513–520.
- Volkman J. K., Eglinton G., Corner E. D. S. and Forsberg T. E. V. (1980) Long-chain alkenes and alkenones in the marine coccolithophorid Emiliania huxleyi. *Phytochemistry* 19, 2619– 2622.
- Wang K. J., Huang Y. and Majaneva M., et al. (2021) Group 2i Isochysidales produce characteristic alkenones reflecting sea ice distribution. *Nat. Commun.*, 1–10.
- Wang L., Longo W. M. and Dillon J. T., et al. (2019) An efficient approach to eliminate steryl ethers and miscellaneous esters/ ketones for gas chromatographic analysis of alkenones and alkenoates. J. Chromatogr. A 1596, 175–182.
- Wara M. W., Ravelo A. C. and Delaney M. L. (2005) Climate change: Permanent El Niño-like conditions during the Pliocene warm period. Science (80-) 309, 758–761.
- White S. M. and Ravelo A. C. (2020) Dampened El Niño in the Early Pliocene Warm Period. *Geophys. Res. Lett.* **47**, 1–10.
- Yamamoto M., Shiraiwa Y. and Inouye I. (2000) Physiological responses of lipids in Emiliania huxleyi and Gephyrocapsa oceanica (Haptophyceae) to growth status and their implications for alkenone paleothermometry. *Org. Geochem.* 31, 799–811
- Zhang Y. G., Pagani M. and Liu Z. (2014) A 12-million-year temperature history of the tropical pacific ocean. *Science* (80-) 344 84-87
- Zhang Y. G., Pagani M. and Wang Z. (2016) Ring Index: A new strategy to evaluate the integrity of TEX86 paleothermometry. *Paleoceanography* 31, 220–232.
- Zheng Y., Heng P. and Conte M. H., et al. (2019) Systematic chemotaxonomic profiling and novel paleotemperature indices based on alkenones and alkenoates: Potential for disentangling mixed species input. *Org. Geochem.* **128**, 26–41.
- Zheng Y., Tarozo R. and Huang Y. (2017) Optimizing chromatographic resolution for simultaneous quantification of long chain alkenones, alkenoates and their double bond positional isomers. Org. Geochem. 111, 136–143.

Associate editor: Jessica Tierney